AGU PUBLICATIONS

Paleoceanography

RESEARCH ARTICLE
10.1002/2017PA003084

Key Points:
- Precipitation over the Parnaíba watershed increased with decreasing AMOC during Heinrich stadial 1
- The ITCZ location over northeastern Brazil changed in proportion to the Atlantic interhemispheric temperature gradient
- Off northeastern Brazil, the highest sediment discharge occurred during the transition from semiarid LGM to the wetter Heinrich stadial 1

Supporting Information:
- Supporting Information S1

Correspondence to:
S. Mulitza,
smulitza@marum.de

Citation:
Mulitza, S., et al. (2017), Synchronous and proportional deglacial changes in Atlantic meridional overturning and northeast Brazilian precipitation, *Paleoceanography*, *32*, 622–633, doi:10.1002/2017PA003084.

Received 11 JAN 2017
Accepted 24 MAY 2017
Accepted article online 27 MAY 2017
Published online 17 JUN 2017

Synchronous and proportional deglacial changes in Atlantic meridional overturning and northeast Brazilian precipitation

Stefan Mulitza[1], Cristiano M. Chiessi[2], Enno Schefuß[1], Jörg Lippold[3], David Wichmann[4], Benny Antz[4], Andreas Mackensen[5], André Paul[1], Matthias Prange[1], Kira Rehfeld[6], Martin Werner[5], Torsten Bickert[1], Norbert Frank[4], Henning Kuhnert[1], Jean Lynch-Stieglitz[7], Rodrigo C. Portilho-Ramos[1,8], André O. Sawakuchi[8], Michael Schulz[1], Tilmann Schwenk[1], Ralf Tiedemann[5], Maximilian Vahlenkamp[1], and Yancheng Zhang[1]

[1]MARUM – Center for Marine Environmental Sciences, University of Bremen, Bremen, Germany, [2]School of Arts, Sciences and Humanities, University of São Paulo, São Paulo, Brazil, [3]Institute of Earth Sciences, University of Heidelberg, Heidelberg, Germany, [4]Institute of Environmental Physics, University of Heidelberg, Heidelberg, Germany, [5]Alfred Wegener Institute, Helmholtz Centre for Polar and Marine Research, Bremerhaven, Germany, [6]Alfred Wegener Institute, Helmholtz Centre for Polar and Marine Research, Potsdam, Germany, [7]School of Earth and Atmospheric Sciences, Georgia Institute of Technology, Atlanta, Georgia, USA, [8]Institute of Geosciences, University of São Paulo, São Paulo, Brazil

Abstract Changes in heat transport associated with fluctuations in the strength of the Atlantic meridional overturning circulation (AMOC) are widely considered to affect the position of the Intertropical Convergence Zone (ITCZ), but the temporal immediacy of this teleconnection has to date not been resolved. Based on a high-resolution marine sediment sequence over the last deglaciation, we provide evidence for a synchronous and near-linear link between changes in the Atlantic interhemispheric sea surface temperature difference and continental precipitation over northeast Brazil. The tight coupling between AMOC strength, sea surface temperature difference, and precipitation changes over northeast Brazil unambiguously points to a rapid and proportional adjustment of the ITCZ location to past changes in the Atlantic meridional heat transport.

1. Introduction

Located close to the southernmost seasonal extension of the intertropical convergence, northeast Brazil is very susceptible to large changes in rainfall on interannual [*Hastenrath*, 2012; *Marengo and Bernasconi*, 2015] to millennial time scales [*Arz et al*., 1998]. Evidence for longer periods of enhanced precipitation during the last glacial period was first provided by sediment layers with increased terrigenous material content deposited on the continental slope off northeast Brazil [*Arz et al*., 1998]. These sediments are characterized by elevated iron/calcium (Fe/Ca) ratios indicating high fluvial input as a consequence of a southward displacement of the ITCZ with AMOC slowdown during Heinrich stadials [*Broccoli et al*., 2006; *Dupont et al*., 2010; *Jennerjahn et al*., 2004; *Wang et al*., 2004]. While continental precipitation over northeast Brazil was clearly increased during Heinrich stadials [*Cruz et al*., 2009; *Dupont et al*., 2010; *Wang et al*., 2004], the relative timing of changes in AMOC, continental precipitation, and terrestrial matter erosion is not well constrained. For example, pollen data covering Heinrich stadial 1 (HS1, from about 18.5 to 15 thousand years B.P.) suggest that the most humid vegetation types in northeast Brazil developed 1–2 thousand years after maximum terrestrial input, associating the highest continental erosion rates with the transition from the semiarid Last Glacial Maximum (LGM) into the wetter HS1 [*Dupont et al*., 2010; *Jennerjahn et al*., 2004], and hence prior to the weakest AMOC state from about 17.5 to 15 kyrs [*McManus et al*., 2004; *Stanford et al*., 2011]. By contrast, peak terrestrial input during earlier Heinrich stadials has been described to occur centuries or even millennia after the associated changes in AMOC [*Burckel et al*., 2015], suggesting a lagged response of continental precipitation and terrestrial discharge to changes in AMOC. The immediacy of the coupling between changes in ocean heat transport and rainfall changes associated to the location of the ITCZ is highly relevant since the AMOC is projected to significantly weaken toward the end of this century [*Collins et al*., 2013].

To minimize some of the inevitable dating uncertainties inherent to time series derived from different paleoclimatic archives and in order to better distinguish between terrestrial matter deposition and precipitation,

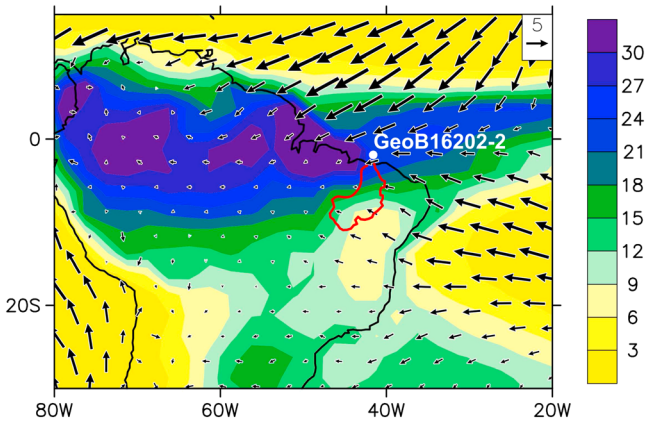

Figure 1. Modern climatological precipitation [*Adler et al.*, 2003] (cm/month) and surface winds [*Kalnay et al.*, 1996] (m/s) for March–May. The Parnaíba River catchment (red) receives peak precipitation during March and April when the Intertropical Convergence Zone is at its southernmost position. White dot marks location of site GeoB16202-2 in front of the Parnaíba River mouth.

we measure proxies of AMOC state ($^{231}Pa/^{230}Th$), continental precipitation (δD of plant wax lipids) and terrestrial matter content (XRF Fe/Ca) in a single marine sediment core taken in front of the Parnaíba catchment, one of the major drainage areas in northeast Brazil. Our data show that continental precipitation over HS1 increased synchronously and proportionally to the reduction in the Atlantic interhemispheric sea surface temperature difference with AMOC slowdown.

2. Materials and Methods

2.1. Core Location, Chronology, and Fe/Ca Ratios

We investigated gravity core GeoB16202-2 (1°54.50′S, 41°35.50′W, 2248 m water depth) [*Mulitza et al.*, 2013] to elucidate the coevolution of continental precipitation, terrestrial matter erosion, and AMOC during the last deglaciation. The neodymium isotopic composition of the terrigenous material from a nearby location [*Zhang et al.*, 2015] identifies suspension load from the Parnaíba River catchment as the principal source for terrestrial sediments deposited at site GeoB16202-2. Rainfall over the Parnaíba catchment is driven by the position of the ITCZ, reaching its southernmost extent over the northern part of the basin in March/April [*Hastenrath*, 2012] (Figure 1).

The age model for gravity core GeoB16202-2 is based on 13 accelerator mass spectrometry radiocarbon dates on planktonic foraminifera (*Globigerinoides ruber* and *Globigerinoides sacculifer*) measured at the Poznań Radiocarbon Laboratory (Table 1). Downcore age uncertainty was modeled using the R script BACON [*Blaauw and Christen*, 2011] version 2.2 and the IntCal13 calibration curve [*Reimer et al.*, 2013] with a reservoir age of 400 ± 200 years (2σ). This uncertainty is close to the range of deglacial surface reservoir ages of 176 to 630 years reconstructed from a nearby core location [*Balmer et al.*, 2016]. BACON was run with default parameter settings, except for a lower autocorrelation or memory (mem.mean set to 0.4) and a flatter prior distribution of the accumulation rate (acc.shape set to 0.5), which allows BACON to adjust the sedimentation rate more flexibly. Ages were modeled using a student *t* distribution, with 9 degrees

Table 1. Radiocarbon Age Control Points for Gravity Core GeoB16202-2[a]

Depth(m)	Core (GeoB)	Lab Code	Conv. Age (Yr B.P.)	Calendar Age Range(2σ, thousand years B.P.)
0.06	16202-2	Poz-49086	1720 ± 35	0.982–1.409
0.50	16202-2	Poz-52734	5695 ± 35	5.773–6.298
1.05	16202-2	Poz-52735	8170 ± 50	8.384–8.976
1.70	16202-2	Poz-52736	10,150 ± 80	10.717–11.601
2.00	16202-2	Poz-49087	10,620 ± 60	11.405–12.395
2.75	16202-2	Poz-52737	11,610 ± 60	12.805–13.288
3.10	16202-2	Poz-52496	12,770 ± 60	14.057–14.999
4.00	16202-2	Poz-49088	13,950 ± 80	15.967–16.762
5.00	16202-2	Poz-52497	14,450 ± 110	16.599–17.501
6.00	16202-2	Poz-49100	14,920 ± 80	17.371–17.997
6.70	16202-2	Poz-52498	15,480 ± 70	18.009–18.608
7.15	16202-2	Poz-52500	18,010 ± 90	20.905–21.699
7.55	16202-2	Poz-52738	20,220 ± 100	23.504–24.210

[a]Sediments were sampled with 10 ml cylindrical syringe (1.5 cm diameter) with cutoff end centered over the given depth.

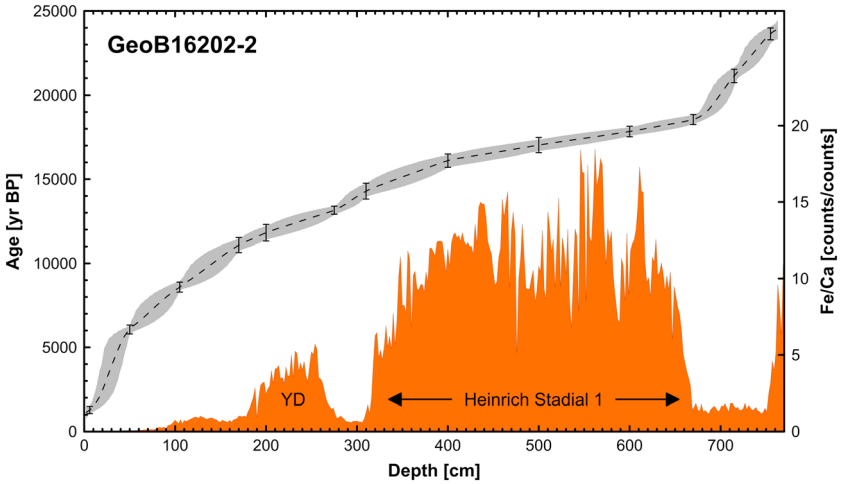

Figure 2. Age-depth relation and uncalibrated Fe/Ca ratios of core GeoB16202-2. Vertical error bars denote 2σ confidence interval of the calibrated calendar ages. Grey shading shows 95% confidence interval around the median age (dashed line) of all age-depth realizations.

of freedom (t.a = 9 and t.b = 10). 10,000 age-depth realizations were obtained to estimate median age and 95% confidence intervals at 1 cm resolution (Figure 2). For $^{231}Pa/^{230}Th$ and δD, 10,000 time series were generated by combining the age-depth models obtained from BACON with 10,000 downcore Monte Carlo proxy realizations within the analytical uncertainty. Confidence intervals were calculated that resulted in 68% and 95% uncertainty envelopes for each proxy at the median ages of the individual sample depths. Note that the measured proxy values can fall on the edges of the 95% uncertainty envelope at local maxima (minima) because a slight temporal shift of the time series in both directions (older or younger) can only lead to a lower (higher) proxy estimation at the same point in time. Finally, 95% uncertainty envelopes for mean sedimentation rates were derived by computing the sedimentation rates between the medians of the calibrated calendar age distributions of the radiocarbon ages for each of the 10,000 age models derived with BACON.

Fe and Ca elemental data were collected with XRF Core Scanner II (AVAATECH Serial No. 2) at MARUM-University of Bremen every 2 cm downcore over a 1.2 cm^2 area with downcore slit size of 10 mm and X-ray tube settings of 10 kV, a current of 0.20 mA, and a sampling time of 20 s at surface of the split core. To avoid contamination and dehydration, the sediment surface was covered with a 4 μm thin SPEXCerti Prep Ultralene1 foil. A Canberra X-PIPS Silicon Drift Detector (SDD; Model SXD 15C-150-500) with 150 eV X-ray resolution, the Canberra Digital Spectrum Analyzer DAS 1000, and an Oxford Instruments 50 W XTF5011 X-Ray tube with rhodium (Rh) target material were used for data acquisition. X-ray spectra were analyzed with the WinAxil software package provided by Canberra Eurisys. Since elemental intensities from XRF scanner measurements are influenced by the water content of the sediment [*Tjallingii et al*., 2007], which may change over time, we excluded Fe/Ca ratios from the Monte Carlo analysis.

2.2. δD and $\delta^{13}C$ Analysis of Plant Wax *n*-Alkanes

Sediment samples were freeze-dried in a Christ Alpha 1-4 LD plus freeze dryer and ground with an agate mortar. Lipids were ultrasonically extracted from 5 to 10 g of dried sediment with an ASE200 accelerated solvent extractor using a dichloromethane:methanol solution (9:1). An internal squalane standard was added prior to extraction. Pipette columns with 4 cm of Na_2SO_4 were used to remove asphaltenes with hexane as solvent. To obtain neutral and acid fractions, the lipid extracts were saponified using 0.1 M KOH in MeOH and neutral lipid extracted with hexane after addition of distilled H_2O. Saturated hydrocarbon fractions were obtained with silica column chromatography by elution with hexane and elution over $AgNO_3$-coated SiO_2 with hexane. Identification of *n*-alkanes was done with a gas chromatography/flame ionization detector (GC/FID) by comparing their retention times to that of an external standard. Concentration of *n*-alkanes was determined by the integration of the chromatogram peak areas

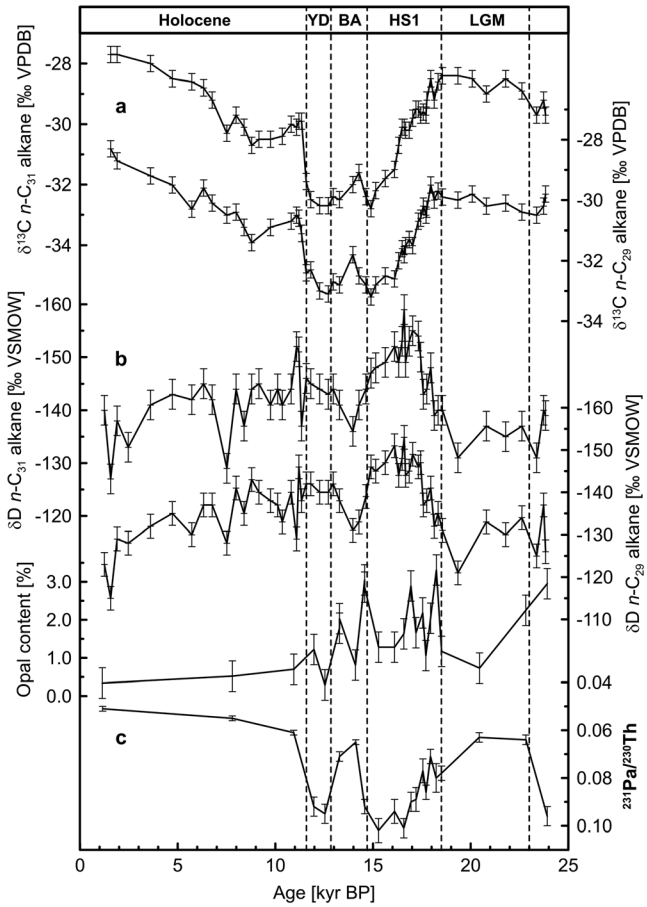

Figure 3. Downcore variability of $\delta^{13}C$, δD, $^{231}Pa/^{230}Th$, and opal content. (a) $\delta^{13}C$ of the C_{31} and C_{29} plant wax *n*-alkanes versus median age scale. (b) δD of the C_{31} and C_{29} plant wax *n*-alkanes uncorrected for ice volume. (c) $^{231}Pa/^{230}Th$ and opal content. Vertical error bars denote 1σ analytical uncertainty. LGM: Last Glacial Maximum; HS1: Heinrich stadial 1, BA: Bølling-Allerød; YD: Younger Dryas.

calibrated against the external standard, composed of a mix of several *n*-alkanes with known concentrations. Extracted blank samples contain only trace amounts of hydrocarbons. Hydrogen isotope analysis of the *n*-C_{29} and *n*-C_{31} alkanes was performed with a ThermoFisher Scientific MAT 253 stable isotope ratio mass spectrometer coupled to a ThermoFisher Scientific Trace gas chromatograph via a GCIsolink interface operated at 1420°C (Table S1 in the supporting information). Hydrogen isotope ratios were measured against calibrated H_2 reference gas and reported in ‰ versus Vienna Standard Mean Ocean Water (VSMOW). The H_3^+ factor was stable during analyses (6.16 ± 0.18 ppm nA^{-1}, n = 51). Stable carbon isotope ratios were determined with a ThermoFinnigan MAT 252 isotope ratio mass spectrometer coupled to a ThermoFisher Scientific Trace gas chromatograph through a GC-C combustion interface with a nickel catalyzer operated at 1000°C. Carbon isotope ratios were measured against calibrated CO_2 reference gas and are reported in ‰ versus Vienna Pee Dee Belemnite (VPDB). Depending on compound abundance, samples were measured at least in duplicate for isotope compositions. The average deviation of the replicates was 2.0‰ for δD and 0.2‰ for $\delta^{13}C$. Analysis of the internal standard squalane (n = 116) yielded an accuracy and precision of 1.4 and 2.3‰ VSMOW for δD and 0.2 and 0.2‰ VPDB for $\delta^{13}C$, respectively. Repeated analyses of an external *n*-alkane standard containing 16 compounds yields long-term standard deviations of 2.8‰ for δD and 0.27‰ for $\delta^{13}C$ measurements (Figures 3a and 3b). Some additional uncertainty can arise from the potential contribution of preaged plant waxes [e.g., *Galy and Eglinton*, 2011], particularly during more arid intervals [*Schefuß et al.*, 2016]. However, the relatively small size of the Parnaíba catchment and the absence of extensive wetlands should contribute to reduce the continental residence time of terrestrial organic matter.

A small correction was applied to δD to account for global ice volume changes [*Schefuß et al*., 2005]. To this end, we converted a benthic oxygen isotope curve [*Waelbroeck et al*., 2002] reflecting mean ocean changes in $\delta^{18}O$ to δD via the global meteoric water line [*Craig*, 1961]. To account for temporal uncertainty, interpolated mean ocean δD values were subtracted from each of the 10,000 age-uncertain δD time series before further calculation of error envelopes.

2.3. Determination of $^{231}Pa/^{230}Th$ and Opal Content

The bulk concentrations of ^{231}Pa, ^{230}Th, ^{232}Th, and ^{238}U have been measured using the inductively coupled plasma-mass spectrometry facilities at the University of Heidelberg (Figure 3c and Table S2) by applying the isotope dilution method and radiochemical standard procedures [*Lippold et al*., 2012a]. The majority of the measurements have been obtained within the scope of the Bachelor thesis by *Wichmann* [2013].

In order to derive the ^{231}Pa and ^{230}Th solely generated by the decay of dissolved ^{235}U and ^{234}U in the overlying water column (the so-called excess fraction, xs) at the time of deposition, $Pa_{xs,0}$ and $Th_{xs,0}$ (where 0 indicates the decay-corrected values) have been calculated from the measured total concentrations of the bulk sediment (Table S3). Uncertainties of the $^{231}Pa/^{230}Th$ ratios are dominated by the uncertainties of the measurements of the ^{231}Pa concentrations which were always better than 1.5% (1σ). Blank corrections were negligible (<0.1%). Isotopic concentrations were calibrated against the reference standard UREM-11 and an in-house ^{231}Pa solution [*Lippold et al*., 2012a].

The corrections for detrital and authigenic contributions to $(^{231}Pa/^{230}Th)_{xs,\ 0}$ followed the method of *Henderson and Anderson* [2003] refined by the suggestions by *Bourne et al.* [2012].

Bourne et al. [2012] noticed that in particular the correction of the detrital (or lithogenic) fraction demands more attention. *Henderson and Anderson* [2003] suggested to quantify Pa_{detr} and Th_{detr} by assuming a constant $(^{238}U/^{232}Th)_{detr}$ in lithogenic material of 0.6 ± 0.1 (activity ratio), which leads (in concert with the ^{232}Th concentration of purely lithogenic origin) to the lithogenic ^{235}U and ^{234}U concentrations. Since the age of lithic material in general exceeds the half-lives of ^{231}Pa and ^{230}Th by far, it can be assumed that radioactive mother and daughter isotopes are in secular equilibrium, resulting in the wanted activities of $^{231}Pa_{detr}$ and $^{230}Th_{detr}$. However, *Bourne et al.* [2012] suggested to define the parameter of $(^{238}U/^{232}Th)_{detr}$ for each location individually, for example, by examining the $^{234}U/^{238}U$ (ingrow of authigenic uranium) or the bulk $^{238}U/^{232}Th$, which at least defines an upper limit on $(^{238}U/^{232}Th)_{detr}$. Further, they suggested the application of a factor of 4% in order to account for the alpha-recoil effect in the sediment grains, which would lower $^{234}U/^{238}U$.

Following this approach, we assumed a $(^{238}U/^{232}Th)_{detr}$ of 0.40 ± 0.03 due to the very low values in bulk $^{238}U/^{232}Th$ observed at this location (minimum 0.37) taking an uncertainty on the $(^{238}U/^{232}Th)_{detr}$ of ±0.03 into account when calculating the error for the $^{231}Pa/^{230}Th$ ratio. We note that at this location the approach by *Bourne et al.* [2012] is crucially necessary, especially for the HS1 interval of our record. When for instance assuming 0.6 for $(^{238}U/^{232}Th)_{detr}$ the extreme input of detrital material would lead to unreasonable values, like $^{231}Pa/^{230}Th > 0.4$.

Opal concentrations were measured on 10–30 mg of dried and homogenized sediment (Figure 3c and Table S4) by automated leaching following the method of *Müller and Schneider* [1993].

2.4. Cross-Correlation Analysis

Pearson's correlation coefficient was estimated for the time series based on the medians of the 10,000 ages simulated for the individual sample depths using a kernel estimator for irregularly sampled time series with an unpublished R translation of the NESToolbox for MATLAB [*Rehfeld and Kurths*, 2014; *Rehfeld et al*., 2011] (Table 2). Time series were detrended with a 5000 year Gaussian high-pass filter to remove orbital-scale variability and deglaciation trends. *P* values for the correlation values were estimated based on the *t* distribution, which is appropriate for small sample sizes. The degrees of freedom were estimated from $DOF_{xy} = \min(\max(N_x,N_y), \max(N_{effx}, N_{effy})) - 2$, where N_x and N_y are the number of observations in the time series *x* and *y*, and N_{effx} and N_{effy} are estimates of the number of independent samples in time series. The effective number of independent observations was estimated based on the ratio of time series range over the decorrelation time. The decorrelation time was estimated from the lag-1 autocorrelation [*Rehfeld and Kurths*, 2014; *Rehfeld et al*., 2011].

Table 2. Pearson Correlation Between Detrended Time Series of Pa/Th, δD, and Atlantic Temperature Difference (ΔSST [*Shakun et al.*, 2012])[a]

	Atlantic Temperature Difference (ΔSST [*Shakun et al.*, 2012])	
	Median Age Model	Ensemble Median (90% range)
Pa/Th	−0.691 ($p < 0.001$)	−0.034 (0.066/−0.143)
$\delta D(C_{29})$	0.401 ($p < 0.001$)	0.187 (0.319/0.053)

[a]Correlation values have been calculated based on the median age model (left column) and for 10,000 Monte Carlo derived proxy time series including age and analytical uncertainty (right column).

To test the unidirectionality of the correlation coefficients across the possible range of age-depth relations, confidence intervals for the correlation coefficients were derived from correlation estimates between time series ensembles (Table 2). The ensembles combine both age uncertainty and proxy uncertainty and yield an ensemble of correlation estimates. To this end, 10,000 age models were combined with 10,000 sets of Monte Carlo derived proxy observations, and correlations were computed as described for the median age model above. Proxy measurement uncertainties were derived from the 1σ analytical uncertainty of each proxy.

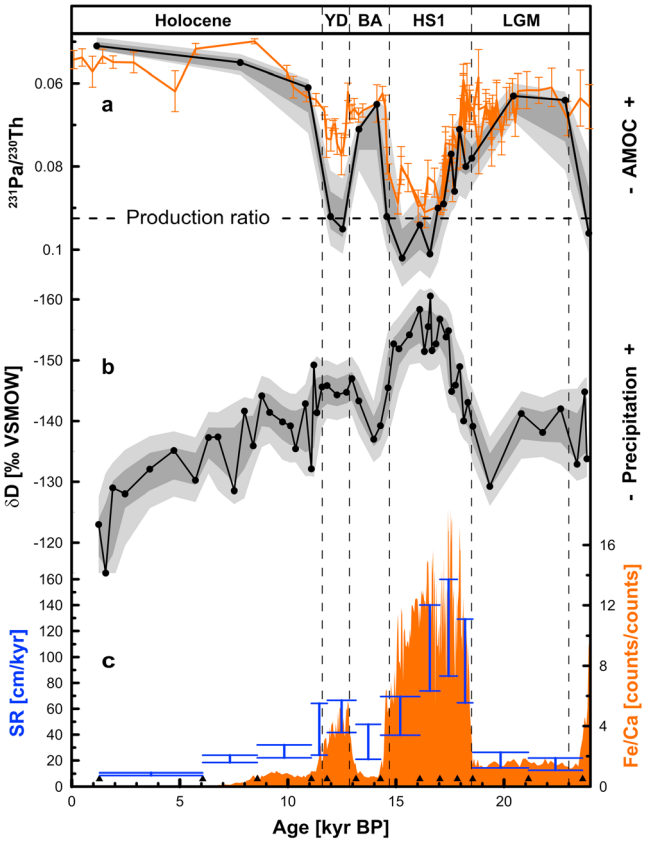

Figure 4. Downcore variability of proxies related to the state of Atlantic meridional overturning circulation (AMOC) and precipitation over northeast Brazil. Grey shading indicates the 68% (dark grey) and 95% (light grey) confidence envelope including age and analytical uncertainty. (a) $^{231}Pa/^{230}Th$ from core GeoB16202-2 (black, this study) and the Bermuda Rise (orange [*Böhm et al.*, 2015; *McManus et al.*, 2004]). (b) Ice volume corrected δD of the *n*-C_{29} alkane of terrestrial plant wax from core GeoB16202-2 (black, this study). (c) Fe/Ca ratio (orange, this study) and 95% confidence range of mean sedimentation rate (SR, blue, this study) between calibrated median calendar ages of radiocarbon datings (triangles). LGM: Last Glacial Maximum; HS1: Heinrich stadial 1, BA: Bølling-Allerød; YD: Younger Dryas.

3. Results

The base of core GeoB16202-2 is dated to an age of about 23.9 thousand years (±0.6) at 763 cm depth (Figure 2). It covers the two most recent phases of increased terrigenous material deposition recorded off northeast Brazil that occurred during HS1 and the Younger Dryas (YD) [*Arz et al.*, 1998]. Both periods are characterized by elevated Fe/Ca ratios (Figure 2) and high sedimentation rates compared to the LGM and the Holocene (Figure 4c). In total, more than 3 m of sediment were deposited during HS1 providing a unique opportunity to trace the coevolution of AMOC and continental precipitation with unprecedented resolution.

We constrained the history of precipitation over the Parnaíba catchment by analyzing the stable hydrogen isotope composition (δD) of plant wax lipids derived from higher plants. The Atomic Energy Agency-Global Network of Isotopes in Precipitation (IAEA-GNIP) stations in northeast Brazil reveal a negative relation between the amount and the stable isotope composition of precipitation [*Vuille et al.*, 2003], suggesting rainfall amount as the principal driver of variations in plant wax δD.

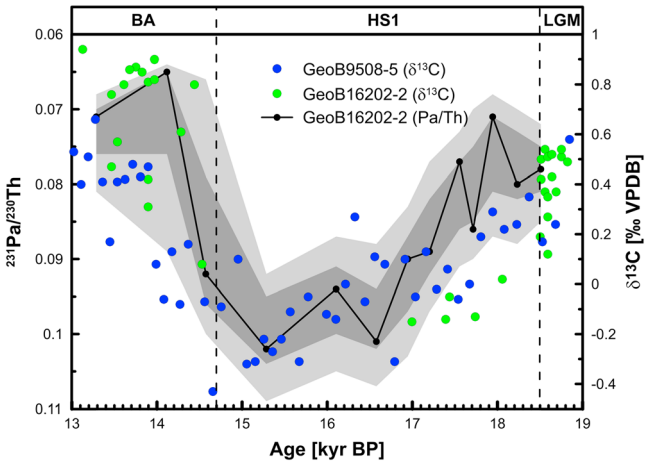

Figure 5. Comparison of Pa/Th ratios and $\delta^{13}C$ of benthic foraminifera over Heinrich stadial 1. Pa/Th from GeoB16202-2 (black dots) is shown with 68% (gray) and 95% (light gray) confidence interval. $\delta^{13}C$ from core GeoB16202-2 (green dots, this study) has been measured on single shells of *Cibicidoides* spp. using standard methods [*Mackensen and Nam*, 2014]. Because epifaunal benthic foraminifera were absent in the second part of HS1 in GeoB16202-2 from about 17 to 14.5 thousand years B.P., we added $\delta^{13}C$ values of *Cibicidoides wuellerstorfi* from eastern Atlantic core GeoB9508-5, (blue dots [*Niedermeyer et al.*, 2009]) from 2384 m water depth. The age model of GeoB9508-5 has been revised as described in section 2.1 and is only based on radiocarbon datings [*Mulitza et al.*, 2008]. Vertical black dashed lines show the lower and upper limits of Heinrich stadial 1. LGM: Last Glacial Maximum; HS1: Heinrich stadial 1, BA: Bølling-Allerød.

High δD of plant wax *n*-alkanes deposited between 23 and 19 thousand years B.P. (mean − 137‰ ± 3) reflects relatively dry conditions in the Parnaíba catchment during the LGM, comparable to the mean late Holocene situation (Figure 4b). During the transition into HS1, from about 18.5 thousand years B.P. onward, δD gradually decreased over a period of about 1.1 thousand years (±0.4) to stabilize around mean δD values of −154‰ (±2) from 17.5 until 15.0 thousand years B.P., the wettest period recorded in GeoB16202-2 during the past ~24 thousand years. This change in δD from the LGM to the second part of HS1 is accompanied by a decrease in $\delta^{13}C$ values of C_{31} and C_{29} plant wax *n*-alkanes of about 3‰, indicative of extensive C3 vegetation in the Parnaíba catchment during the second part of HS1 compared to the LGM (Figure 3a). A change in vegetation type can influence the sedimentary plant wax δD composition through different hydrogen isotope fractionation factors of C3 and C4 plants [e.g., *Sachse et al.*, 2012]. Since C3 trees have on average higher δD values than C4 grasses [*Sachse et al.*, 2012], resulting in higher δD values of wax lipids from C3 trees for the same isotope signature of precipitation, the change toward lower δD during HS1 in our record cannot be explained by a change in vegetation type. At present, the exact fractionation factors of plant types in NE Brazil are not known; based on the African C3/C4 end-members, however, we estimate that a change in vegetation type could not account for more than 3–4‰ attenuation of the δD signal over HS1 in GeoB16202-2, which is minor relative to the total amplitude of changes.

δD sharply increased at the onset of the Bølling-Allerød interstadial after about 14.7 thousand years B.P. (±0.5) and returned to wetter conditions with a δD minimum at 12.9 thousand years B.P. (±0.4), close to the onset of the YD at 12.7 thousand years B.P. [*Brauer et al.*, 2008] (Figure 4). The following Holocene section of GeoB16202-2 is characterized by increasing δD values indicating a progressive aridification of the Parnaíba catchment from about 11 thousand years B.P. toward the late Holocene.

We infer the covariation of precipitation over the Parnaíba catchment and AMOC in core GeoB16202-2 from sedimentary $^{231}Pa/^{230}Th$. Due to the different particle affinities and hence residence times of Pa and Th produced from U decay in seawater, the decay-corrected ratio of $^{231}Pa/^{230}Th$ is used as a proxy for the strength of the AMOC [*McManus et al.*, 2004]. In agreement with previously published records from the western [*Böhm et al.*, 2015; *McManus et al.*, 2004] and eastern North Atlantic [*Gherardi et al.*, 2005], $^{231}Pa/^{230}Th$ indicates a marked slowdown of the AMOC during HS1 and the YD (Figure 4a). While the general trends of the $^{231}Pa/^{230}Th$ downcore profiles from GeoB16202-2 (2248 m water depth) and from the North Atlantic (>3000 m water depth) are very similar, the absolute values recorded in GeoB16202-2 during HS1 and YD are slightly higher. One reason why $^{231}Pa/^{230}Th$ records from two different sites within more or less the same water mass may feature different values is the downstream buildup of the ^{231}Pa concentration in the dissolved phase. Due to the deep export from the North Atlantic the dissolved ^{231}Pa concentration is increasing on its path toward the South Atlantic [*Luo et al.*, 2010; *Marchal et al.*, 2000] leading to higher $^{231}Pa/^{230}Th$ downstream at GeoB16202-2 compared to the North Atlantic records. Furthermore, biogenic opal has been shown to act as a strong scavenger of Pa [*Chase et al.*, 2002]

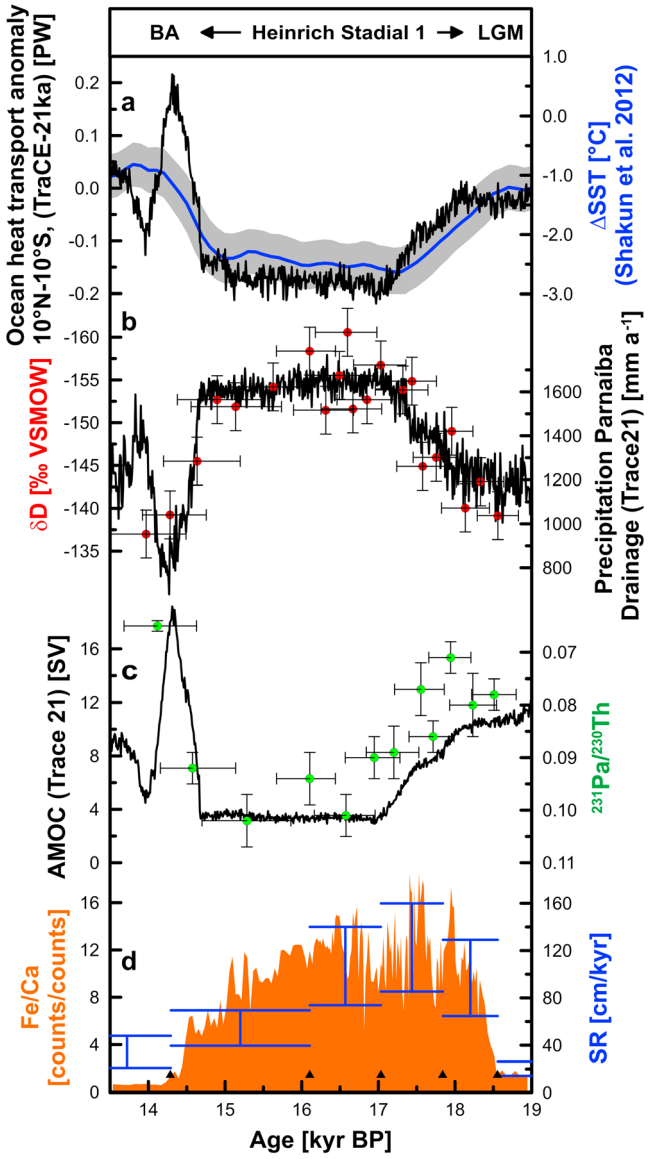

Figure 6. Modeled (TraCE-21ka [*He*, 2011; *Liu et al.*, 2009]) and reconstructed evolution of AMOC, Atlantic temperature gradient, and precipitation over Heinrich stadial 1. Vertical error bars denote measurement uncertainty (±1σ), horizontal error bars age uncertainty (95% range). (a) Reconstructed (blue [*Shakun et al.*, 2012]) annual mean temperature difference between North and South Atlantic and modeled (black [*He*, 2011; *Liu et al.*, 2009; *Yang et al.*, 2015]) ocean heat transport anomaly relative to 22 thousand years B.P. (b) Ice volume corrected δD of n-C_{29} alkane of terrestrial plant wax from core Geo16202-2 (red dots, this study) and modeled annual mean precipitation over the Parnaíba River catchment (black [*Liu et al.*, 2009]). (c) $^{231}Pa/^{230}Th$ from core GeoB16202-2 (green circles, this study) and modeled maximum Atlantic meridional overturning (black [*Liu et al.*, 2009]). (d) Fe to Ca ratio (red, uncalibrated counts) and 95% confidence range of mean sedimentation rate (blue, this study) between calibrated median calendar ages of radiocarbon datings (triangles, this study).

potentially influencing $^{231}Pa/^{230}Th$ on local scales. However, given opal contents below 4% in core GeoB16202-2 (Figure 3c), a dominant effect of opal production on $^{231}Pa/^{230}Th$ seems unlikely, consistent with basin-wide compilations [*Bradtmiller et al.*, 2014; *Lippold et al.*, 2012b; *Lippold et al.*, 2016].

4. Discussion

Generally, the overall deglacial evolution of precipitation recorded in GeoB16202-2 agrees with proxies from cave [*Cruz et al.*, 2009] and lake [*Jacob et al.*, 2007] deposits in northeast Brazil, supporting our interpretation that δD variations were primarily driven by changes in rainfall amount. A change in summer insolation has been identified as a major forcing of Holocene changes in precipitation over northeast Brazil and likely explains the gradual early to late Holocene increase in our δD record through adjustments in large-scale atmospheric subsidence over northeast Brazil [*Cruz et al.*, 2009]. The covariation of δD with $^{231}Pa/^{230}Th$ ratios during HS1 and the YD, however, suggests a prominent role of ocean circulation for the modulation of continental precipitation over the Parnaíba catchment during the last deglaciation. The AMOC reduction during HS1 and the YD diminished the northward oceanic heat transport across the equator and therefore cooled the North Atlantic and warmed the South Atlantic in a bipolar seesaw [e.g., *Barker et al.*, 2009; *Marino et al.*, 2015; *Mix et al.*, 1986; *Shakun et al.*, 2012]. The correlation between detrended time series of $^{231}Pa/^{230}Th$ from core GeoB16202-2 and the interhemispheric Atlantic sea surface temperature (SST) difference [*Shakun et al.*, 2012] is indeed significant ($r = -0.69$, $p < 0.001$), when the age model based on the medians of the calendar age distributions is considered. The confidence interval for the correlation coefficients, however, suggests that the correlation is not significantly different from zero over the entire range of the modeled ensemble of the $^{231}Pa/^{230}Th$ time series (Table 2). This is likely a result of the large uncertainty of

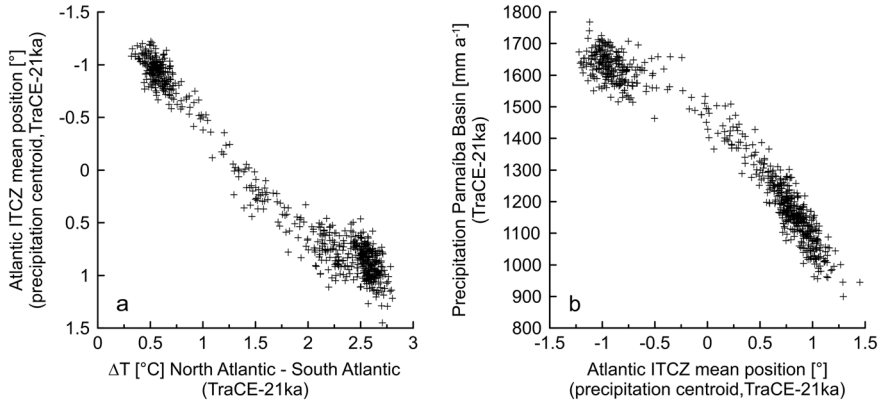

Figure 7. Modeled relation between Atlantic hemispheric temperature difference, Atlantic ITCZ mean position, and annual precipitation above the Parnaíba catchment from TraCE-21ka [*He*, 2011], http://www.cgd.ucar.edu/ccr/TraCE/) over Heinrich stadial 1 from 21.8 to 14.9 thousand years B.P. (a) Modeled relation between Atlantic surface temperature difference and ITCZ location. (b) Relation between ITCZ location and precipitation over the Parnaíba catchment. The ITCZ location is the latitude of the centroid over the Atlantic Ocean between 50°W and 20°E calculated from the area-integrated annual mean precipitation from 15°S to 15°N as described in *Frierson and Hwang* [2012]. The Atlantic temperature difference is the area-integrated surface temperature difference between North Atlantic (Arctic Circle to equator) and the South Atlantic (Antarctic Circle to equator) between 68°W and 20°E. TraCE-21ka sea surface temperature and precipitation have been downloaded from https://www.earthsystemgrid.org/project/nnhtml.

$^{231}Pa/^{230}Th$ ratios that allows a large variability in the $^{231}Pa/^{230}Th$ time series ensemble in combination with a relatively low temporal resolution. Additional evidence for a change in deep-ocean circulation during HS1 comes from the carbon isotope composition of epifaunal benthic foraminifera (Figure 5). Increasing $^{231}Pa/^{230}Th$ values at the onset of HS1 were accompanied by decreasing benthic $\delta^{13}C$ values, consistent with a reduced ventilation of the deep Atlantic Ocean [*Lynch-Stieglitz et al*., 2014].

Our δD data suggest that deglacial changes in oceanic heat transport (Figure 6a) controlled precipitation over the Parnaíba catchment (Figure 6b). Mechanisms to explain the relation between ITCZ location and Atlantic overturning invoke the interplay between atmospheric and oceanic heat transport [*Broccoli et al*., 2006; *Chiang and Friedman*, 2012; *Frierson et al*., 2013; *Marshall et al*., 2014]. At present, the cross-equatorial heat transport of about 0.5 petawatt (PW) by the AMOC leads to a sea surface temperature maximum north of the equator, heating of the Northern Hemisphere atmosphere, and a mean ITCZ location in the Northern Hemisphere, allowing the upper limb of the southern Hadley Cell to transport energy back into the Southern Hemisphere [*Frierson et al*., 2013]. The strong AMOC allows the ITCZ to only seasonally reach northeast Brazil, promoting its modern-day semiarid climate [*Hastenrath*, 2012]. The reduction of the AMOC during HS1 and the YD cooled the North Atlantic and the overlying atmosphere, shifting the thermal equator to the south (Figure 6a). The resulting southward shift of the ITCZ led to increased precipitation over the Parnaíba catchment (Figure 6b). Indeed, we find a significant correlation ($r = 0.40$, $p < 0.001$) between the detrended time series of the Atlantic interhemispheric temperature difference [*Shakun et al*., 2012] and the δD record from core GeoB16202-2 (Table 2).

The synchrony of Atlantic interhemispheric temperature difference, mean ITCZ location, and precipitation over the Parnaíba catchment is supported by the results of the TraCE-21 ka project, simulating the transient climate evolution over the last deglaciation [*Liu et al*., 2009]. In this simulation, a slowdown of the AMOC (Figure 6c), forced by meltwater input into the North Atlantic, leads to a decrease in the northward oceanic heat transport [*Yang et al*., 2015] (Figure 6a). The resulting change in the SST gradient between North and South Atlantic is associated with a southward progression of the Atlantic ITCZ of approximately 1° latitude per °C (Figure 7a) and a synchronous increase of precipitation over the Parnaíba catchment (Figure 6b). The proportionality between ITCZ location and precipitation over the Parnaíba catchment (Figure 7b) demonstrates a consistent relationship between total precipitation received by the Parnaíba catchment and the mean position of the ITCZ. Both model data (Figure 8a) and δD of plant wax lipids from GeoB16202-2 (Figure 8b) provide clear evidence for a synchronous and proportional linkage of precipitation over the Parnaíba catchment to changes in the Atlantic SST distribution.

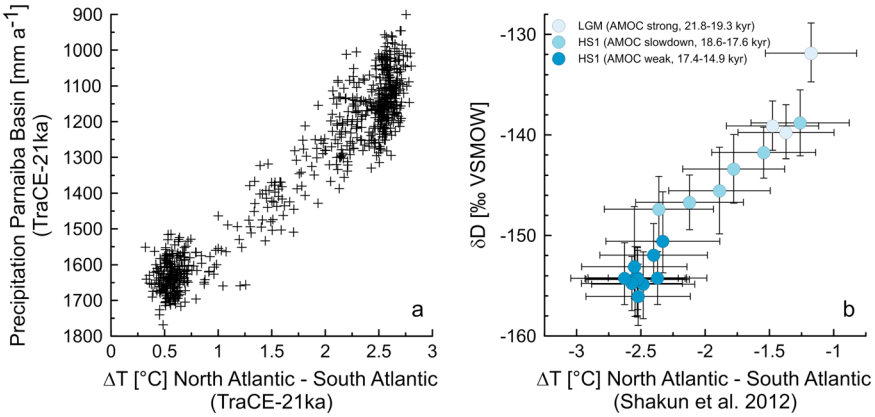

Figure 8. Relation between Atlantic interhemispheric temperature difference and precipitation over northeast Brazil and δD of plant wax from core GeoB16202-2 from 21.8 to 14.9 thousand years B.P. (a) Modeled (TraCE-21ka) relation between annual mean precipitation over the Parnaíba River catchment and Atlantic interhemispheric surface temperature difference [*He*, 2011; *Liu et al*., 2009]. (b) Relation between δD of *n*-C_{29} alkane of terrestrial plant wax (this study) and Atlantic temperature gradient [*Shakun et al*., 2012]. Error bars denote 68% confidence intervals derived from age and analytical uncertainty.

Our data also clarify conflicting evidence in the timing of changes in AMOC, continental rainfall, and terrigenous input off northeast Brazil. The $^{231}Pa/^{230}Th$ data indicate a two-phase evolution of the AMOC during HS1 with an initial gradual slowdown phase from about 18.5 to 17.5 thousand years B.P., followed by a phase of weak AMOC from about 17.5 to 15.0 thousand years B.P. (Figure 4c). Fe/Ca ratios and bulk sedimentation rates from our core show the highest sediment discharge during the slowdown phase, not in the second, wettest phase of HS1. This early response of terrestrial sediment deposition can be explained by the effects of changing vegetation cover [*Dupont et al*., 2010; *Jennerjahn et al*., 2004]. During the early transitional phase of HS1, highly variable precipitation [*Cruz et al*., 2009] led to high sediment discharge due to increased runoff and mobilization of soils in the still sparsely vegetated watershed. Declining erosion and suspension input followed in the second phase of HS1, when rain forests and gallery forests spread and tree ferns suggest perennial humid conditions [*Dupont et al*., 2010; *Jennerjahn et al*., 2004]. A change toward a more tree-dominated vegetation over HS1 is also consistent with continuously decreasing $\delta^{13}C$ values of plant wax *n*-alkanes (Figure 3a), indicating a shift to dominant C3 vegetation in the Parnaíba catchment in the second phase of HS1, which led to soil stabilization.

5. Conclusions

Our data show that precipitation over the Parnaíba catchment was increased during HS1 and the YD compared to today and the LGM with the highest sediment discharge at the onset of HS1. The close relations of δD of plant wax lipids to $^{231}Pa/^{230}Th$ and the Atlantic SST distribution suggest that the precipitation changes were caused by migrations of the ITCZ driven by changes in the strength of the AMOC. Modeling studies suggest that the relation between the Atlantic temperature gradient and the ITCZ location is nearly linear over a wide range of time scales [*Donohoe et al*., 2013; *McGee et al*., 2014]. The apparent linearity between changes in δD of plant wax from the Parnaíba catchment and reconstructed SST gradient over HS1 indicates that this relation is indeed a robust feature of Atlantic ocean-atmosphere interaction. Any future asymmetrical warming of the Atlantic Ocean surface, for example, due to a slowdown of the AMOC [*Collins et al*., 2013], would likely lead to a corresponding shift in the position of the ITCZ and related tropical rainfall with potentially large socioeconomic impacts [*Hastenrath*, 2012] on semiarid areas adjacent to the modern seasonal ITCZ range.

Acknowledgments
Constructive comments by two anonymous referees greatly improved the paper. This work was funded through the DFG Research Center/Cluster of Excellence "The Ocean in the Earth System" and by the Helmholtz Climate Initiative REKLIM. Radiocarbon dating was performed at Poznan Radiocarbon Laboratory. Thanks to U. Röhl, R. Kreutz, V. Lukies, M. Klann, and T. Westerhold for technical support. This research used data acquired at the XRF Core Scanner Lab at the MARUM—Center for Marine Environmental Sciences, University of Bremen, Germany. We thank B. Otto-Bliesner, Z. Liu, and F. He for making the TraCE-21ka model output available via the Earth System Grid (National Center for Atmospheric Research). C.M.C. acknowledges financial support from FAPESP (grant 2012/17517-3). Financial support was provided by the Deutsche Forschungsgemeinschaft through grants Ma821/43 and Fr1341/6 to B.A. and through grant Li1815/4 to J.L. Data are available at www.pangaea.de.

References

Adler, R. F., et al. (2003), The version-2 Global Precipitation Climatology Project (GPCP) monthly precipitation analysis (1979-present), *J. Hydrometeorol.*, *4*(6), 1147–1167, doi:10.1175/1525-7541(2003)004<1147:tvgpcp>2.0.co;2.

Arz, H. W., J. Pätzold, and G. Wefer (1998), Correlated millennial-scale changes in surface hydrography and terrigenous sediment yield inferred from last-glacial marine deposits off northeastern Brazil, *Quat. Res.*, *50*(2), 157–166, doi:10.1006/qres.1998.1992.

Balmer, S., M. Sarnthein, M. Mudelsee, and P. M. Grootes (2016), Refined modeling and ^{14}C plateau tuning reveal consistent patterns of glacial and deglacial ^{14}C reservoir ages of surface waters in low-latitude Atlantic, *Paleoceanography*, *31*, 1030–1040, doi:10.1002/2016PA002953.

Barker, S., P. Diz, M. J. Vautravers, J. Pike, G. Knorr, I. R. Hall, and W. S. Broecker (2009), Interhemispheric Atlantic seesaw response during the last deglaciation, *Nature*, *457*(7233), 1097–1102, doi:10.1038/nature07770.

Blaauw, M., and A. J. Christen (2011), Flexible paleoclimate age-depth models using an autoregressive gamma process, *Bayesian Anal.*, *6*(3), 457–474, doi:10.1214/11-ba618.

Böhm, E., J. Lippold, M. Gutjahr, M. Frank, P. Blaser, B. Antz, J. Fohlmeister, N. Frank, M. B. Andersen, and M. Deininger (2015), Strong and deep Atlantic meridional overturning circulation during the last glacial cycle, *Nature*, *517*(7532), 73–76, doi:10.1038/nature14059.

Bourne, M. D., A. L. Thomas, C. Mac Niocaill, and G. M. Henderson (2012), Improved determination of marine sedimentation rates using $^{230}Th_{xs}$, *Geochem. Geophys. Geosyst.*, *13*, Q09017, doi:10.1029/2012GC004295.

Bradtmiller, L. I., J. F. McManus, and L. F. Robinson (2014), $^{231}Pa/^{230}Th$ evidence for a weakened but persistent Atlantic meridional overturning circulation during Heinrich Stadial 1, *Nat. Commun.*, *5*, doi:10.1038/ncomms6817.

Brauer, A., G. H. Haug, P. Dulski, D. M. Sigman, and J. F. W. Negendank (2008), An abrupt wind shift in western Europe at the onset of the Younger Dryas cold period, *Nat. Geosci.*, *1*(8), 520–523, doi:10.1038/ngeo263.

Broccoli, A. J., K. A. Dahl, and R. J. Stouffer (2006), Response of the ITCZ to Northern Hemisphere cooling, *Geophys. Res. Lett.*, *33*, L01702, doi:10.1029/2005GL024546.

Burckel, P., C. Waelbroeck, J. M. Gherardi, S. Pichat, H. Arz, J. Lippold, T. Dokken, and F. Thil (2015), Atlantic Ocean circulation changes preceded millennial tropical South America rainfall events during the last glacial, *Geophys. Res. Lett.*, *42*, 411–418, doi:10.1002/2014GL062512.

Chase, Z., R. F. Anderson, M. Q. Fleisher, and P. W. Kubik (2002), The influence of particle composition and particle flux on scavenging of Th, Pa and Be in the ocean, *Earth Planet. Sci. Lett.*, *204*(1–2), 215–229, doi:10.1016/S0012-821X(02)00984-6.

Chiang, J. C. H., and A. R. Friedman (2012), Extratropical Cooling, Interhemispheric Thermal Gradients, and Tropical Climate Change, *Annu. Rev. Earth Planet. Sci.*, *40*, 383–412, doi:10.1146/annurev-earth-042711-105545.

Collins, M., et al. (2013), Long-term climate change: Projections, commitments and irreversibility, in *Climate Change 2013: The Physical Science Basis. Contribution of Working Group I to the Fifth Assessment Report of the Intergovernmental Panel on Climate Change*, edited by T. F. Stocker et al., pp. 1029–1136, Cambridge Univ. Press, Cambridge, U. K., and New York.

Craig, H. (1961), Isotopic variations in meteoric waters, *Science*, *133*(346), 1702–1703, doi:10.1126/science.133.3465.1702.

Cruz, F. W., M. Vuille, S. J. Burns, X. Wang, H. Cheng, M. Werner, R. L. Edwards, I. Karmann, A. S. Auler, and H. Nguyen (2009), Orbitally driven east-west antiphasing of South American precipitation, *Nat. Geosci.*, *2*(3), 210–214, doi:10.1038/ngeo444.

Donohoe, A., J. Marshall, D. Ferreira, and D. McGee (2013), The relationship between ITCZ location and cross-equatorial atmospheric heat transport: From the seasonal cycle to the Last Glacial Maximum, *J. Clim.*, *26*(11), 3597–3618, doi:10.1175/jcli-d-12-00467.1.

Dupont, L. M., F. Schlütz, C. T. Ewah, T. C. Jennerjahn, A. Paul, and H. Behling (2010), Two-step vegetation response to enhanced precipitation in Northeast Brazil during Heinrich event 1, *Global Change Biol.*, *16*(6), 1647–1660, doi:10.1111/j.1365-2486.2009.02023.x.

Frierson, D. M. W., and Y.-T. Hwang (2012), Extratropical influence on ITCZ shifts in slab ocean simulations of global warming, *J. Clim.*, *25*(2), 720–733, doi:10.1175/jcli-d-11-00116.1.

Frierson, D. M. W., Y.-T. Hwang, N. S. Fuckar, R. Seager, S. M. Kang, A. Donohoe, E. A. Maroon, X. Liu, and D. S. Battisti (2013), Contribution of ocean overturning circulation to tropical rainfall peak in the Northern Hemisphere, *Nat. Geosci.*, *6*(11), 940–944, doi:10.1038/ngeo1987.

Galy, V., and T. Eglinton (2011), Protracted storage of biospheric carbon in the Ganges-Brahmaputra basin, *Nat. Geosci.*, *4*(12), 843–847, doi:10.1038/ngeo1293.

Gherardi, J. M., L. Labeyrie, J. F. McManus, R. Francois, L. C. Skinner, and E. Cortijo (2005), Evidence from the northeastern Atlantic basin for variability in the rate of the meridional overturning circulation through the last deglaciation, *Earth Planet. Sci. Lett.*, *240*(3–4), 710–723, doi:10.1016/j.epsl.2005.09.061.

Hastenrath, S. (2012), Exploring the climate problems of Brazil's Nordeste: A review, *Clim. Change*, *112*(2), 243–251, doi:10.1007/s10584-011-0227-1.

He, F. (2011), Simulating Transient Climate Evolution of the Last Deglaciation With CCSM3, PhD thesis, 171 pp., Univ. of Wisconsin-Madison.

Henderson, G. M., and R. F. Anderson (2003), The U-series toolbox for paleoceanography, *Rev. Mineral. Geochem.*, *52*, 493–531, doi:10.2113/0520493.

Jacob, J., Y. Huang, J.-R. Disnar, A. Sifeddine, M. Boussafir, A. L. Spadano Albuquerque, and B. Turcq (2007), Paleohydrological changes during the last deglaciation in northern Brazil, *Quat. Sci. Rev.*, *26*(7–8), 1004–1015, doi:10.1016/j.quascirev.2006.12.004.

Jennerjahn, T. C., V. Ittekkot, H. W. Arz, H. Behling, J. Pätzold, and G. Wefer (2004), Asynchronous terrestrial and marine signals of climate change during Heinrich events, *Science*, *306*(5705), 2236–2239, doi:10.1126/science.1102490.

Kalnay, E., et al. (1996), The NCEP/NCAR 40-year reanalysis project, *Bull. Am. Meteorol. Soc.*, *77*(3), 437–471, doi:10.1175/1520-0477(1996)077<0437:tnyrp>2.0.co;2.

Lippold, J., S. Mulitza, G. Mollenhauer, S. Weyer, D. Heslop, and M. Christl (2012a), Boundary scavenging at the East Atlantic margin does not negate use of $^{231}Pa/^{230}Th$ to trace Atlantic overturning, *Earth Planet. Sci. Lett.*, *333*, 317–331, doi:10.1016/j.epsl.2012.04.005.

Lippold, J., Y. M. Luo, R. Francois, S. E. Allen, J. Gherardi, S. Pichat, B. Hickey, and H. Schulz (2012b), Strength and geometry of the glacial Atlantic meridional overturning circulation, *Nat. Geosci.*, *5*(11), 813–816, doi:10.1038/ngeo1608.

Lippold, J., M. Gutjahr, P. Blaser, E. Christner, M. L. de Carvalho Ferreira, S. Mulitza, M. Christl, F. Wombacher, E. Böhm, and B. Antz (2016), Deep water provenance and dynamics of the (de)glacial Atlantic meridional overturning circulation, *Earth Planet. Sci. Lett.*, *445*, 68–78.

Liu, Z., et al. (2009), Transient simulation of last deglaciation with a new mechanism for Bølling-Allerød warming, *Science*, *325*(5938), 310–314, doi:10.1126/science.1171041.

Luo, Y., R. Francois, and S. E. Allen (2010), Sediment $^{231}Pa/^{230}Th$ as a recorder of the rate of the Atlantic meridional overturning circulation: Insights from a 2-D model, *Ocean Sci.*, *6*(1), 381–400.

Lynch-Stieglitz, J., M. W. Schmidt, L. G. Henry, W. B. Curry, L. C. Skinner, S. Mulitza, R. Zhang, and P. Chang (2014), Muted change in Atlantic overturning circulation over some glacial-aged Heinrich events, *Nat. Geosci.*, *7*(2), 144–150, doi:10.1038/ngeo2045.

Mackensen, A., and S.-I. Nam (2014), Taxon-specific epibenthic foraminiferal $\delta^{18}O$ in the Arctic Ocean: Relationship to water masses, deep circulation, and brine release, *Mar. Micropaleontol.*, *113*, 34–43, doi:10.1016/j.marmicro.2014.09.002.

Marchal, O., R. Francois, T. F. Stocker, and F. Joos (2000), Ocean thermohaline circulation and sedimentary $^{231}Pa/^{230}Th$ ratio, *Paleoceanography*, *15*(6), 625–641, doi:10.1029/2000PA000496.

Marengo, J. A., and M. Bernasconi (2015), Regional differences in aridity/drought conditions over Northeast Brazil: Present state and future projections, *Clim. Change*, *129*(1–2), 103–115, doi:10.1007/s10584-014-1310-1.

Marino, G., E. J. Rohling, L. Rodriguez-Sanz, K. M. Grant, D. Heslop, A. P. Roberts, J. D. Stanford, and J. Yu (2015), Bipolar seesaw control on last interglacial sea level, *Nature*, *522*(7555), 197–201, doi:10.1038/nature14499.

Marshall, J., A. Donohoe, D. Ferreira, and D. McGee (2014), The ocean's role in setting the mean position of the Inter-Tropical Convergence Zone, *Clim. Dyn.*, *42*(7–8), 1967–1979, doi:10.1007/s00382-013-1767-z.

McGee, D., A. Donohoe, J. Marshall, and D. Ferreira (2014), Changes in ITCZ location and cross-equatorial heat transport at the Last Glacial Maximum, Heinrich Stadial 1, and the mid-Holocene, *Earth Planet. Sci. Lett.*, *390*, 69–79, doi:10.1016/j.epsl.2013.12.043.

McManus, J. F., R. Francois, J. M. Gherardi, L. D. Keigwin, and S. Brown-Leger (2004), Collapse and rapid resumption of Atlantic meridional circulation linked to deglacial climate changes, *Nature*, *428*(6985), 834–837, doi:10.1038/nature02494.

Mix, A. C., W. F. Ruddiman, and A. McIntyre (1986), Late Quaternary paleoceanography of the tropical Atlantic, 1: Spatial variability of annual mean sea-surface temperatures, 0-20,000 years B.P, *Paleoceanography*, *1*(1), 43–66, doi:10.1029/PA001i001p00043.

Mulitza, S., M. Prange, J. B. Stuut, M. Zabel, T. von Dobeneck, A. C. Itambi, J. Nizou, M. Schulz, and G. Wefer (2008), Sahel megadroughts triggered by glacial slowdowns of Atlantic meridional overturning, *Paleoceanography*, *23*, PA4206, doi:10.1029/2008PA001637.

Mulitza, S., C. M. Chiessi, A. P. S. Cruz, T. Frederichs, J. G. Gomes, M. H. D. C. Gurgel, J. Haberkern, E. Huang, L. Jovane, and H. Kuhnert (2013), Response of Amazon sedimentation to deforestation, land use and climate variability—Cruise No. MSM20/3—February 19–March 11, 2012—Recife (Brazil)—Bridgetown (Barbados), 86 pp., DFG-Senatskommission für Ozeanographie, Bremen.

Müller, P. J., and R. Schneider (1993), An automated leaching method for the determination of opal in sediments and particulate matter, *Deep-Sea Res. Part I-Oceanogr. Res. Pap.*, *40*(3), 425–444, doi:10.1016/0967-0637(93)90140-x.

Niedermeyer, E. M., M. Prange, S. Mulitza, G. Mollenhauer, E. Schefuss, and M. Schulz (2009), Extratropical forcing of Sahel aridity during Heinrich stadials, *Geophys. Res. Lett.*, *36*, L20707, doi:10.1029/2009GL039687.

Rehfeld, K., and J. Kurths (2014), Similarity estimators for irregular and age-uncertain time series, *Clim. Past*, *10*(1), 107–122, doi:10.5194/cp-10-107-2014.

Rehfeld, K., N. Marwan, J. Heitzig, and J. Kurths (2011), Comparison of correlation analysis techniques for irregularly sampled time series, *Nonlinear Process. Geophys.*, *18*(3), 389–404, doi:10.5194/npg-18-389-2011.

Reimer, P. J., et al. (2013), IntCal13 and Marine13 radiocarbon age calibration curves 0–50,000 years cal BP, *Radiocarbon*, *55*(4), 1869–1887.

Sachse, D., et al. (2012), Molecular Paleohydrology: Interpreting the Hydrogen- Isotopic Composition of Lipid Biomarkers from Photosynthesizing Organisms, *Annu. Rev. Earth Planet. Sci.*, *40*, 221–249, doi:10.1146/annurev-earth-042711-105535.

Schefuß, E., S. Schouten, and R. R. Schneider (2005), Climatic controls on central African hydrology during the past 20,000 years, *Nature*, *437*(7061), 1003–1006, doi:10.1038/nature03945.

Schefuß, E., T. I. Eglinton, C. L. Spencer-Jones, J. Rullkotter, R. De Pol-Holz, H. M. Talbot, P. M. Grootes, and R. R. Schneider (2016), Hydrologic control of carbon cycling and aged carbon discharge in the Congo River basin, *Nat. Geosci.*, *9*(9), 687–690, doi:10.1038/ngeo2778.

Shakun, J. D., P. U. Clark, F. He, S. A. Marcott, A. C. Mix, Z. Liu, B. Otto-Bliesner, A. Schmittner, and E. Bard (2012), Global warming preceded by increasing carbon dioxide concentrations during the last deglaciation, *Nature*, *484*(7392), 49–54, doi:10.1038/nature10915.

Stanford, J. D., E. J. Rohling, S. Bacon, A. P. Roberts, F. E. Grousset, and M. Bolshaw (2011), A new concept for the paleoceanographic evolution of Heinrich event 1 in the North Atlantic, *Quat. Sci. Rev.*, *30*(9–10), 1047–1066, doi:10.1016/j.quascirev.2011.02.003.

Tjallingii, R., U. Röhl, M. Kolling, and T. Bickert (2007), Influence of the water content on X-ray fluorescence core-scanning measurements in soft marine sediments, *Geochem. Geophys. Geosyst.*, *8*, Q02004, doi:10.1029/2006GC001393.

Vuille, M., R. S. Bradley, M. Werner, R. Healy, and F. Keimig (2003), Modeling $\delta^{18}O$ in precipitation over the tropical Americas: 1. Interannual variability and climatic controls, *J. Geophys. Res.*, *108*(D6), 4174, doi:10.1029/2001JD002038.

Waelbroeck, C., L. Labeyrie, E. Michel, J. C. Duplessy, J. F. McManus, K. Lambeck, E. Balbon, and M. Labracherie (2002), Sea-level and deep water temperature changes derived from benthic foraminifera isotopic records, *Quat. Sci. Rev.*, *21*(1–3), 295–305, doi:10.1016/s0277-3791(01)00101-9.

Wang, X. F., A. S. Auler, R. L. Edwards, H. Cheng, P. S. Cristalli, P. L. Smart, D. A. Richards, and C. C. Shen (2004), Wet periods in northeastern Brazil over the past 210 kyr linked to distant climate anomalies, *Nature*, *432*(7018), 740–743, doi:10.1038/nature03067.

Wichmann, D. (2013), Untersuchung der Ozeanzirkulation vor Brasilien bis ins letzte Glazial mittels $^{231}Pa/^{230}Th$, BSc thesis, 34 pp., Univ. of Heidelberg.

Yang, H. J., Y. Y. Zhao, Z. Y. Liu, Q. Li, F. He, and Q. Zhang (2015), Heat transport compensation in atmosphere and ocean over the past 22,000 years, *Sci. Rep.*, *5*, doi:10.1038/srep16661.

Zhang, Y., C. M. Chiessi, S. Mulitza, M. Zabel, R. I. F. Trindade, M. H. B. M. Hollanda, E. L. Dantas, A. Govin, R. Tiedemann, and G. Wefer (2015), Origin of increased terrigenous supply to the NE South American continental margin during Heinrich Stadial 1 and the Younger Dryas, *Earth Planet. Sci. Lett.*, *432*, 493–500.